Title: From red to green luminescence via surface functionalization. Effect of 2-(5-mercaptothien-2-yl)-8-(thien-2-yl)-5-hexylthieno[3,4-c]pyrrole-4,6-dione ligands on the photoluminescence of alloyed Ag-In-Zn-S nanocrystals

Author: Patrycja Kowalik, Piotr Bujak, Zbigniew Wróbel, Mateusz Penkala, Kamil Kotwica, Anna Maroń, Adam Pron

Citation style: Kowalik Patrycja, Bujak Piotr, Wróbel Zbigniew, Penkala Mateusz, Kotwica Kamil, Maroń Anna, Pron Adam. (2020). From red to green luminescence via surface functionalization. Effect of 2-(5-mercaptothien-2-yl)-8-(thien-2-yl)-5-hexylthieno[3,4-c]pyrrole-4,6-dione ligands on the photoluminescence of alloyed Ag-In-Zn-S nanocrystals. "Inorganic Chemistry" Vol. 59, iss. 19 (2020), s. 14594–14604, doi 10.1021/acs.inorgchem.0c02468

Inorganic Chemistry

pubs.acs.org/IC Article

From Red to Green Luminescence via Surface Functionalization. Effect of 2-(5-Mercaptothien-2-yl)-8-(thien-2-yl)-5-hexylthieno[3,4-*c*]pyrrole-4,6-dione Ligands on the Photoluminescence of Alloyed Ag−In−Zn−S Nanocrystals

Patrycja Kowalik,* Piotr Bujak,* Zbigniew Wróbel, Mateusz Penkala, Kamil Kotwica, Anna Maroń, and Adam Pron

Cite This: *Inorg. Chem.* 2020, 59, 14594−14604

Read Online

ACCESS | Metrics & More | Article Recommendations | Supporting Information

ABSTRACT: A semiconducting molecule containing a thiol anchor group, namely 2-(5-mercaptothien-2-yl)-8-(thien-2-yl)-5-hexylthieno-[3,4-*c*]pyrrole-4,6-dione (abbreviated as D-A-D-SH), was designed, synthesized, and used as a ligand in nonstoichiometric quaternary nanocrystals of composition $Ag_{1.0}In_{3.1}Zn_{1.0}S_{4.0}(S_{6.1})$ to give an inorganic/organic hybrid. Detailed NMR studies indicate that D-A-D-SH ligands are present in two coordination spheres in the organic part of the hybrid: (i) inner in which the ligand molecules form direct bonds with the nanocrystal surface and (ii) outer in which the ligand molecules do not form direct bonds with the inorganic core. Exchange of the initial ligands (stearic acid and 1-aminooctadecane) for D-A-D-SH induces a distinct change of the photoluminescence. Efficient red luminescence of nanocrystals capped with initial ligands (λ_{max} = 720 nm, quantum yield = 67%) is totally quenched and green luminescence characteristic of the ligand appears (λ_{max} = 508 nm, quantum yield = 10%). This change of the photoluminescence mechanism can be clarified by a combination of electrochemical and spectroscopic investigations. It can be demonstrated by cyclic voltammetry that new states appear in the hybrid as a consequence of D-A-D-SH binding to the nanocrystals surface. These states are located below the nanocrystal LUMO and above its HOMO, respectively. They are concurrent to deeper donor and acceptor states governing the red luminescence. As a result, energy transfer from the nanocrystal HOMO and LUMO levels to the ligand states takes place, leading to effective quenching of the red luminescence and appearance of the green one.

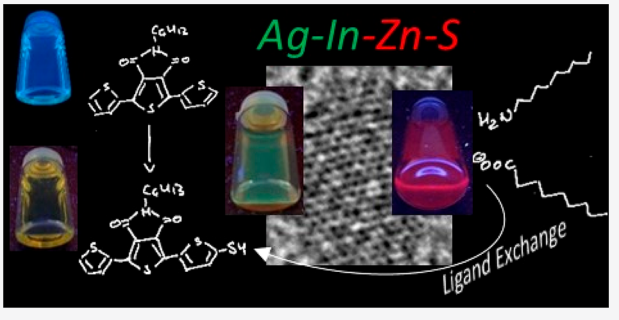

INTRODUCTION

Semiconductor nanocrystals can be considered as inorganic/organic hybrids consisting of an inorganic core and surfacial capping ligands which ensure their colloidal stability. Primary surfacial ligands, that is, ligands introduced during the nanocrystals synthesis, can be further modified or exchanged for new ligands providing a desired functionality.[1−8] Detailed studies of the interactions at the inorganic core−ligands interface are of crucial importance since they determine basic physical properties of the resulting hybrids. There are numerous literature examples of the effect of ligands and nanocrystal core compositions on their energy gap, positions of valence and conduction bands, photoluminescence, and their quantum yields (QYs).[9−14] Hybrids containing ligands of organic semiconductor nature are especially interesting since they can exhibit tunable photo- and electroactivity.[2,15−21] Potential capping ligands can be searched among low and high molecular mass electroactive compounds whose ionization potential (IP), electron affinity (EA), band gap, absorption, and emission spectra can be tuned by appropriate functionalization. Moreover, many of them can be processed from popular solvents.[22−24] However, the overwhelming majority of organic electroactive compounds do not contain appropriate functional groups capable of binding to the nanocrystal surface. Such functionalization is necessary because the preparations of classical blends by mixing nonfunctionalized organic semiconductors with inorganic nanocrystals frequently lead to uncontrollable phase separation.[25] Thus, new designs of electroactive molecules have to be elaborated if they are planned to serve as nanocrystals capping ligands, involving, among others, introduction of alkyl-type solubilizing groups and functional groups which could form stable bonds with nanocrystal core surfacial atoms (ions).[2]

Received: August 18, 2020
Published: September 17, 2020

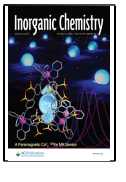

https://dx.doi.org/10.1021/acs.inorgchem.0c02468
Inorg. Chem. 2020, 59, 14594−14604

It should be noted that, to date, the vast majority of papers devoted to the design of functional ligands and the ligand exchange dealt with nanocrystals of binary semiconductors such as CdSe, CdS, PbSe, and PbS. Recent progress in the synthesis of ternary and quaternary nanocrystals, including strongly nonstoichiometric alloyed ones, has not induced parallel intensive research on the design of "tailor-made" photo- and electroactive ligands suitable for these nanocrystals as well as on the exchange of primary ligands for functionalized ones. This type of research is highly desirable in the case of quaternary Ag−In−Zn−S nanocrystals, especially, because by changing their composition it is possible to tune their efficient luminescence over the whole visible spectral range. This strongly facilitates their application in electronics[26−29] and biomedical sciences.[30−35] The analysis of ligand exchange-induced photoluminescence changes is especially important in this respect. In the case of binary CdSe nanocrystals the luminescence is governed by the classical radiative recombination mechanism 1S(e) → 1S(h). On the contrary, the luminescence of alloyed quaternary Ag−In−Zn−S nanocrystals proceeds via the donor−acceptor radiative recombination mechanism, associated with the presence of point defects in the nanocrystal core.[36]

In this report, we describe the design and fabrication of a hybrid consisting of the quaternary Ag−In−Zn−S core capped with organic semiconductor-type ligands, namely, 2-(5-mercaptothien-2-yl)-8-(thien-2-yl)-5-hexylthieno[3,4-*c*]-pyrrole-4,6-dione. Spectroscopic and electrochemical properties of this hybrid are analyzed. We also demonstrate that the exchange of primary, spectroscopically inactive ligands for the conjugated ones induces a hypsochromic shift of the photoluminescence peak by over 200 nm, that is, from the red region of the spectrum to the green one.

RESULTS AND DISCUSSION

The presented research was focused on surface functionalization of alloyed Ag−In−Zn−S with photo- and electroactive ligands. In our previous research we elaborated new procedures of fabricating these quaternary nanoparticles of different compositions which exhibited strong and tunable photoluminescence covering green and red regions of the spectrum (QY in the range 48−67%).[37−39] We also developed an efficient method of exchanging primary hydrophobic ligands for hydrophilic ones such as 11-mercaptoundecanoic acid (MUA), for example. In subsequent steps bioactive objects could be grafted to these capping ligands such as transferrin, doxorubicin, unsymmetrical bisacridine derivatives, and so on, providing new hybrids suitable for medical applications.[34,35]

Ag−In−Zn−S nanocrystals studied in this research were prepared by using a reaction mixture that consisted of silver nitrate, indium(III) chloride, zinc stearate, and 1-dodecanethiol (DDT) dissolved in 1-octadecene (ODE) in molar ratios $AgNO_3/InCl_3$/zinc stearate/DDT = 1.0/3.4/3.6/5.6. To initiate the reaction, sulfur dissolved in oleylamine (S/OLA) was injected to this mixture at 150 °C.[38,39] The resulting nanoparticles were spherical in shape (diameter, d = 5.8 ± 0.9 nm) and showed the composition of $Ag_{1.0}In_{3.1}Zn_{1.0}S_{4.0}(S_{6.1})$ as determined by EDS (the value in parentheses indicates the stoichiometric content of sulfur with respect to the content of Ag, In, and Zn; for EDS data see Figure S1). Additional characterization was performed by using XPS (see Figure S2 where the survey and high-resolution (Ag 3d, In 3d, Zn 2p, and S 2p) spectra are presented). The recorded spectra are characteristic of alloyed Ag−In−Zn−S nanocrystals and consistent with our previous findings.[38,39] They emitted red light (λ_{max} = 720 nm, QY = 67%).

In Figure 1, a powder diffractogram of $Ag_{1.0}In_{3.1}Zn_{1.0}S_{4.0}(S_{6.1})$ nanocrystals is presented together

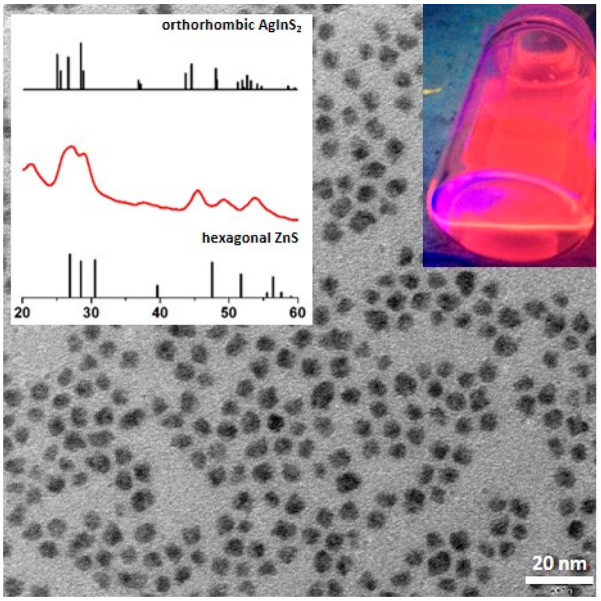

Figure 1. TEM image of $Ag_{1.0}In_{3.1}Zn_{1.0}S_{4.0}(S_{6.1})$ nanocrystals (d = 5.8 ± 0.9 nm, n = 200). An XRD pattern of these nanocrystals is presented in the inset.

with their representative TEM image. The alloyed nature of the obtained nanocrystals was confirmed by the positions of the observed Bragg reflections which were intermediate between these characteristic of orthorhombic $AgInS_2$ (JCPDS 00-025-1328) and those of hexagonal ZnS (JCPDS 00-036-1450). Broadening of the registered peaks was consistent with small size of the prepared nanocrystals clearly evidenced by TEM. Additionally, in Figure S3 a representative HR-TEM image of the obtained nanocrystals is presented together with a histogram showing their size distribution.

Primary ligands were identified by using a procedure previously elaborated by our group and consisting of controlled dissolution of the nanocrystals inorganic core and NMR analysis of the organic residue.[40] The obtained ^{1}H NMR spectrum (see Figure S4) revealed the presence of two types of ligands: stearic acid originating from the precursor of zinc and 1-aminooctadecane formed through hydrogenation of OLA in the course of the preparation of nanocrystals.[39]

Among organic semiconductors, which could be considered as candidates for photo- and electroactive surfacial ligands of inorganic semiconductors nanocrystals, donor−acceptor compounds deserve a special attention. This is due to the fact that their band gap as well as HOMO and LUMO energies can be precisely tuned by selection of donor and acceptor units of appropriate strength. In particular, increasing the accepting ability of "A" units results in lowering of the LUMO level, whereas strengthening of the electron donating effect of "D" units results in rising of the HOMO level.[20,22,41−43]

As an electro- and photoactive ligand we selected thieno-[3,4-*c*]pyrrole-4,6-dione (TPD), which was used as a building block in numerous low[44−46] and high molecular weight organic semiconductors.[47−52] A strong advantage of TPD is associated

https://dx.doi.org/10.1021/acs.inorgchem.0c02468
Inorg. Chem. 2020, 59, 14594−14604

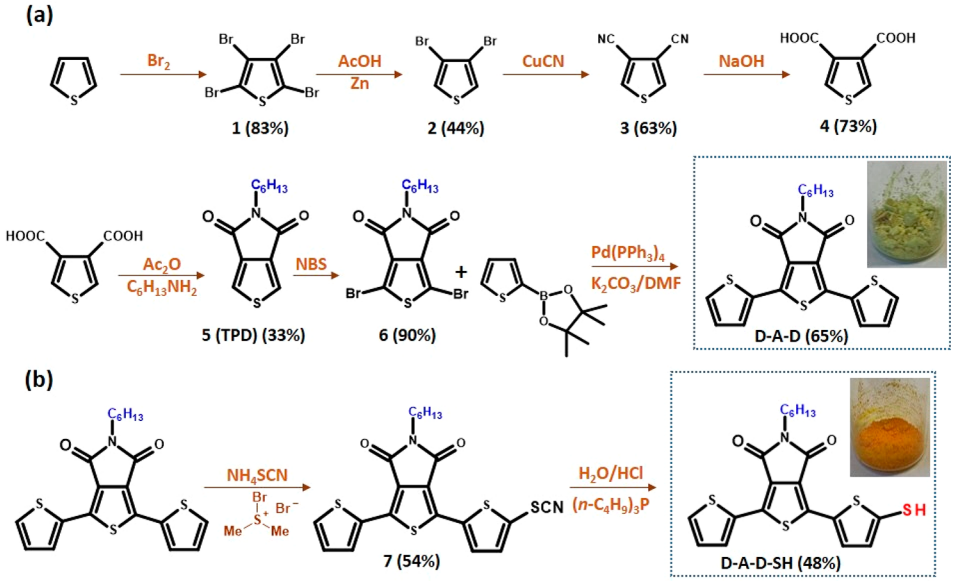

Figure 2. Chemical structures of the (a) 2,8-bis(thien-2-yl)-5-hexylthieno[3,4-*c*]pyrrole-4,6-dione (D-A-D) and (b) electroactive ligand 2-(5-mercaptothien-2-yl)-8-(thien-2-yl)-5-hexylthieno[3,4-*c*]pyrrole-4,6-dione (D-A-D-SH) and their synthetic pathways.

with the presence of an alkyl group in the dione subunit which increases its solubility and stability as a ligand. Functionalization of this molecule with two thienyl groups at 2- and 8-positions yielded a donor−acceptor−donor compound, 2,8-bis(thien-2-yl)-5-hexylthieno[3,4-*c*]pyrrole-4,6-dione, abbreviated in the subsequent text as D-A-D. This molecule contained no anchor functional group capable of binding to the nanocrystal surface; therefore, it was additionally functionalized with a thiol group (−SH). The selection of this functional group was rationalized by the versatility of this anchor group with respect to semiconductor nanocrystals synthesis. In addition, it assured a stable bond with the nanocrystal surficial atoms. An amine anchor group could in principle be considered as an alternative. However, the binding capability of a given amine depends on its basicity; that is, more basic aliphatic amines form stronger bonds than aromatic ones which are weaker bases.[40] Introduction of a $-CH_2NH_2$ group to D-A-D would lead to efficient binding of the ligand to the nanocrystal surface, but at the same time the presence of a methylene group would result in a conjugation break between the nanocrystal and the ligand. Thus, a thiol-functionalized semiconductor ligand, namely 2-(5-mercaptothien-2-yl)-8-(thien-2-yl)-5-hexylthieno[3,4-*c*]pyrrole-4,6-dione (D-A-D-SH), better provided the anchoring capability while retaining the conjugation.

Two methods of the synthesis of thieno[3,4-*c*]pyrrole-4,6-dione (TPD) have been developed to date. In the classical approach thiophene is used as the starting substrate.[53,54] Alternatively, the Gewald reaction can be used for the preparation of an appropriate thiophene derivative which upon condensation yields the target product.[55] In the research presented here the classical method was used for the preparation of D-A-D (Figure 2a). Thiophene was first transformed into thiophene-3,4-dicarboxylic acid, which upon condensation with an aliphatic amine (e.g., n-$C_6H_{13}NH_2$) yielded the core of TPD. The detailed procedure of the TPD core preparation can be found in the Supporting Information. Bromination of this core using NBS followed by Suzuki coupling with thiophene-2-boronic acid pinacol ester yielded D-A-D.[56] D-A-D was transformed into its thiol derivative, namely 2-(5-mercaptothien-2-yl)-8-(thien-2-yl)-5-hexylthieno-[3,4-*c*]pyrrole-4,6-dione (D-A-D-SH) (Figure 2b), in a two-step process. In the first step −SCN was introduced by using NH_4SCN/bromodimethylsulfonium bromide[57] and then transformed into −SH in the presence of H_2O/HCl.[58]

Chemical identities of D-A-D and D-A-D-SH were confirmed by NMR spectroscopy. In particular, the ^{1}H NMR spectrum of D-A-D revealed the presence of a triplet at 3.55 ppm corresponding to the CH_2N moiety. In the aromatic part of the spectrum three doublets appeared at 6.65, 6.73, and 8.13 ppm which could be ascribed to protons of the thienyl rings. Two characteristic signals at 38.6 and 162.4 ppm, present in the ^{13}C NMR spectrum, could unequivocally be attributed to the CH_2N and C═O groups of the acceptor unit. Detailed analysis of ^{1}H and ^{13}C NMR data, including ^{1}H−^{1}H COSY and ^{1}H−^{13}C HMQC results, is presented in Figure S5. Functionalization of D-A-D with −SH to yield D-A-D-SH perturbs its symmetry. As a result, in the ^{1}H NMR spectrum two additional doublets appear at 6.93 and 7.87 ppm originating from coupling of thienyl protons with that of the thiol group (J = 3.9 Hz). Because the second thienyl ring remains unsubstituted, its protons give rise to three doublets at 6.64, 6.74, and 8.11 ppm. In Figure S6, the ^{1}H and ^{1}H−^{1}H COSY NMR spectra of D-A-D-SH are presented together with detailed signals attributions. Introduction of −SH to (D-A-D) significantly reduces the solubility of the resulting D-A-D-SH. For this reason no good quality ^{13}C NMR spectrum of this compound could be registered.

The target inorganic/organic hybrid, that is, Ag−In−Zn−S/D-A-D-SH, was obtained through exchange of primary ligands for D-A-D-SH. In all preparations $Ag_{1.0}In_{3.1}Zn_{1.0}S_{4.0}(S_{6.1})$ nanocrystals originating from the same batch were used (see the Experimental Section for a detailed description of the ligand exchange). The ligand exchange had no effect on the nanocrystals size (d = 6.0 ± 0.8 nm) as well as on the composition of the inorganic core ($Ag_{1.0}In_{3.1}Zn_{1.0}S_{4.0}(S_{6.1})$ (see Figure S7 for their TEM image and EDS spectrum).

https://dx.doi.org/10.1021/acs.inorgchem.0c02468
Inorg. Chem. 2020, 59, 14594−14604

Upon ligand exchange the colloidal stability of the studied nanocrystals remained essentially unchanged despite limited solubility of free D-A-D-SH as compared to D-A-D. This can be considered as a manifestation of the formation of a stable bond between the nanocrystal surface $Ag_{1.0}In_{3.1}Zn_{1.0}S_{4.0}(S_{6.1})$ and D-A-D-SH which affects the ligand polarity and facilitates the dispersion of the resulting nanohybrids in nonpolar or weakly polar solvents.

For the identification of the chemical nature of ligands and their mode of binding to nanocrystals, diffusion-ordered NMR or nuclear Overhauser effect spectroscopies are used.[59] Their efficacy was proven in the analysis of binding of amine- or acid-type ligands to several binary nanocrystals such as CdS, CdSe, and CdTe.[60,61] In this research we propose a different approach based on the analysis of ^{1}H and ^{13}C NMR and $^{1}H-^{1}H$ COSY and $^{1}H-^{13}C$ HMQC spectra presented in Figures S8 and S9. In the ^{1}H NMR spectrum registered in C_6D_6, two signals characteristic of D-A-D-SH, namely triplets at 3.53 and 3.95 ppm, attributable to the CH_2N group, could be distinguished. In Figure 3, aliphatic regions of the ^{1}H NMR spectra of D-A-D and D-A-D-SH are compared with those of Ag−In−Zn−S/D-A-D-SH recorded after 16 and 128 scans, respectively. The presence of these two above-mentioned peaks indicates that two types of ligands coexist in the hybrid: (i) strongly bound to the nanocrystal surface (chemical shift ∼3.9 ppm) and (ii) ligands from the second (outer) coordination sphere whose chemical shift (∼3.5 ppm) is close to that registered for "free" D-A-D-SH ligands. The coexistence of two coordination spheres is further corroborated by the evolution of the spectrum of Ag−In−Zn−S/D-A-D-SH with increasing number of scans. Upon its increase from 16 to 128, the $I_{3.9ppm}/I_{3.5ppm}$ signals ratio decreases from ca. 1/2 to ca. 1/9. This distinct difference is caused by different protons relaxation times for these two types of ligands. Protons of surface-bound ligands (∼3.9 ppm) relax more slowly as compared to protons of free ligands (∼3.5 ppm). If the pulse repeat sequence is kept constant (1 s), each particular pulse excites a smaller number of nuclei in the surface-bound ligands as compared to ligands of the second coordination sphere. Upon increasing repetition of pulses, this difference grows giving rise to a decrease of the $I_{3.9ppm}/I_{3.5ppm}$ ratio. A similar effect is also observed for other NMR signals of the aromatic region, registered for Ag−In−Zn−S/D-A-D-SH. The signal at 7.91 ppm corresponds to protons of the thienyl group in the ligand bound to the nanocrystal surface, whereas the doublet at 7.87 ppm is attributed to the corresponding protons in ligands of the second coordination sphere. The $I_{7.91ppm}/I_{7.87ppm}$ ratio decreases from 1/5 for 16 scans to 1/27 for 128 scans (Figure S9).

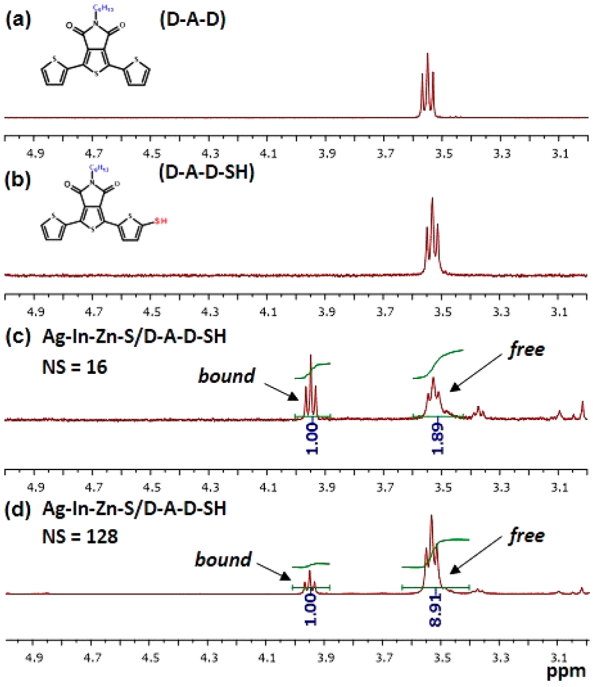

Figure 3. ^{1}H NMR spectra (in the range 3.0−5.0 ppm) of the 2,8-bis(thien-2-yl)-5-hexylthieno[3,4-*c*]pyrrole-4,6-dione (D-A-D) (a), 2-(5-mercaptothien-2-yl)-8-(thien-2-yl)-5-hexylthieno[3,4-*c*]pyrrole-4,6-dione (D-A-D-SH) (b), and hybrid Ag−In−Zn−S/D-A-D-SH recorded with 16 scans (c) and 128 scans (d) in benzene-d_6 at 298 K.

The presented results unequivocally show that a fraction of D-A-D-SH molecules form direct bonds with the nanocrystal surface (first coordination sphere). The second coordination sphere consists of D-A-D-SH molecules which do not form direct bonds with the $Ag_{1.0}In_{3.1}Zn_{1.0}S_{4.0}(S_{6.1})$ nanocrystals inorganic core. The coexistence of two (inner and outer) coordination spheres has previously been reported for other types of ligand-stabilized nanocrystals.[62]

In a detailed study electrochemical and spectroscopic properties of the hybrid Ag−In−Zn−S/D-A-D-SH) were compared with those determined for the same nanocrystals ($Ag_{1.0}In_{3.1}Zn_{1.0}S_{4.0}(S_{6.1})$) capped with primary ligands, the organic semiconductor (D-A-D), and its derivative containing the anchor group (D-A-D-SH).

In Figure 4 a representative cyclic voltammogram of $Ag_{1.0}In_{3.1}Zn_{1.0}S_{4.0}(S_{6.1})$ nanocrystals capped with primary ligands (stearic acid and 1-aminooctane) and dispersed in 0.1 M Bu_4NBF_4/CH_2Cl_2 is presented. The observed oxidation and reduction processes are irreversible. From the potentials of the oxidation (1.28 V vs Fc/Fc^+) and reduction (−1.49 V vs Fc/Fc^+) onsets the ionization potential (IP) and electron affinity (EA) can be calculated knowing the potential of the Fc/Fc^+ redox couple on the absolute potential scale (eqs 1 and 2):[63−65]

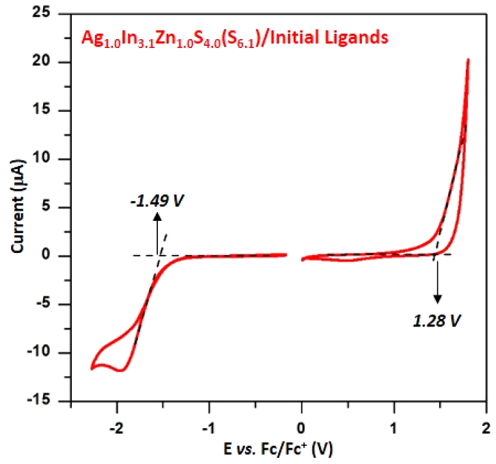

Figure 4. Cyclic voltammograms of $Ag_{1.0}In_{3.1}Zn_{1.0}S_{4.0}(S_{6.1})$ nanocrystals capped with initial ligands (stearic acid and 1-aminooctadecane). Electrolyte: 0.1 M Bu_4NBF_4/CH_2Cl_2, reference electrode Ag/0.1 M $AgNO_3$ in acetonitrile, scan rate = 50 mV/s.

https://dx.doi.org/10.1021/acs.inorgchem.0c02468
Inorg. Chem. 2020, 59, 14594−14604

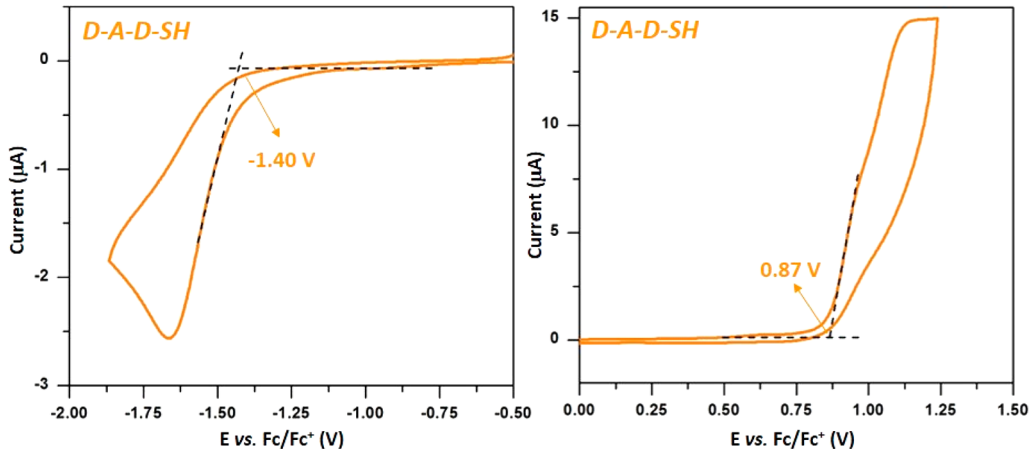

Figure 5. Cyclic voltammograms of 2-(5-mercaptothien-2-yl)-8-(thien-2-yl)-5-hexylthieno[3,4-*c*]pyrrole-4,6-dione (D-A-D-SH). Electrolyte: 0.1 M Bu_4NBF_4/CH_2Cl_2, reference electrode Ag/0.1 M $AgNO_3$ in acetonitrile, scan rate = 50 mV/s.

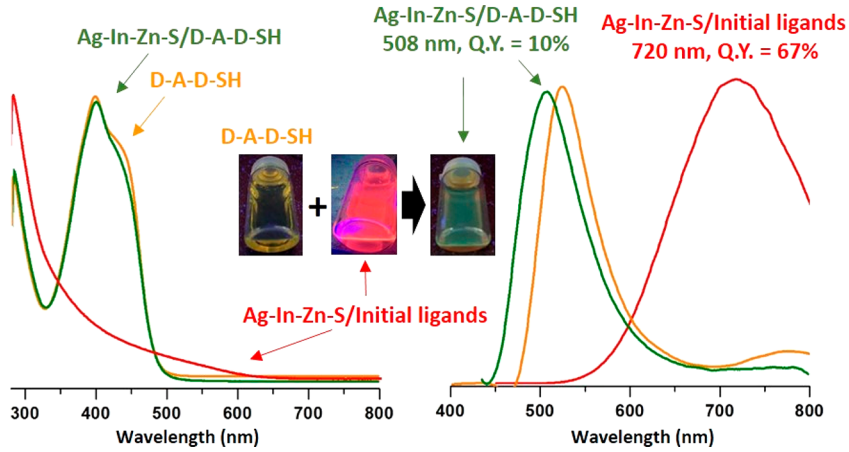

Figure 6. UV−vis−NIR (left column) and photoluminescence (right column) spectra of 2-(5-mercaptothien-2-yl)-8-(thien-2-yl)-5-hexylthieno[3,4-*c*]pyrrole-4,6-dione (D-A-D-SH) (orange lines), Ag−In−Zn−S capped with initial ligands (red lines), and ligand (D-A-D-SH) (green lines) in toluene.

$$\text{IP (eV)} = |e|(E_{\text{ox(onset)}} + 4.8) \quad (1)$$

$$\text{EA (eV)} = -|e|(E_{\text{red(onset)}} + 4.8) \quad (2)$$

IP and EA values determined for $Ag_{1.0}In_{3.1}Zn_{1.0}S_{4.0}(S_{6.1})$ capped with primary ligands are 6.1 and −3.3 eV, respectively, which correspond to an electrochemical band gap Eg_{el} = 2.8 eV.

The optical band gap of the same nanocrystals, Eg_{opt}, was determined from their UV−vis−NIR spectrum by using the relationship $(Ah\nu)^2$ vs $h\nu$ (Figure S10). The obtained value of 2.60 eV is lower than the electrochemical one. This difference originates from Coulombic interactions between the created charges; thus $Eg_{el} = Eg_{opt} + \Delta E_J$ (where ΔE_J is the Coulombic interaction energy).[66] The value of ΔE_J = 0.2 eV obtained for $Ag_{1.0}In_{3.1}Zn_{1.0}S_{4.0}(S_{6.1})$ capped with primary ligands is in the typical range for the majority of inorganic semiconductor nanocrystals.[67] The measured value of the optical band gap (Eg_{opt} = 2.60 eV) is mainly governed by the nanocrystals nonstoichiometric composition ($Ag_{1.0}In_{3.1}Zn_{1.0}S_{4.0}(S_{6.1})$) and in particular by the Ag/In and Ag/Zn ratios. The quantum confinement effect also interferes. The gap is significantly larger than that of stoichiometric macrocrystalline $AgInS_2$ (Eg_{opt} = 1.98 eV).[68−70] The upper edge of its valence band corresponds to a hybrid of S 3p and Ag 4d orbitals hybrid, whereas its lower edge to In 5s5p hybridized with S 3p orbitals.[71] A decrease of the Ag/In ratio to ca. 0.3 in nonstoichiometric Ag−In−S nanocrystals results in lowering of the valence band and an increase of the band gap.[72] The band gap of macrocrystalline hexagonal ZnS is equal to 3.68 eV.[73] Thus, an increase of the Ag/Zn ratio in Ag−In−Zn−S quaternary nanocrystals (to ∼1.0 in the nanocrystals described in this research) results in an increase of the band gap. To sum up, a combination of all phenomena described above leads to widening of the band gap, which in the case of $Ag_{1.0}In_{3.1}Zn_{1.0}S_{4.0}(S_{6.1})$ nanocrystals reaches 2.60 eV.

$Ag_{1.0}In_{3.1}Zn_{1.0}S_{4.0}(S_{6.1})$ nanocrystals capped with primary ligands (stearic acid and 1-aminooctadecane) emit red light (λ_{max} = 720 nm, QY = 67%). The photoluminescence of alloyed Ag−In−Zn−S nanocrystals does not follow the simple radiative recombination 1S(e) → 1S(h) mechanism, known for CdSe nanocrystals, for example. The observed large values of the Stokes shift ∼170 nm and the FWHM (full width at half-maximum) of the photoluminescence peak seem to indicate the donor−acceptor mechanism of radiative recombination in this type of nanocrystal.[36]

The same set of characterization techniques was applied to D-A-D-SH, the second component of the investigated hybrid. In Figure 5 representative cyclic voltammograms, registered in

https://dx.doi.org/10.1021/acs.inorgchem.0c02468
Inorg. Chem. 2020, 59, 14594−14604

the negative (vs Fc/Fc^+) and positive potential ranges, are presented. D-A-D-SH undergoes irreversible oxidation and irreversible reduction. The potentials of the reduction and oxidation onsets are used for the determination of IP and EA according to eqs 1 and 2. The reduction of D-A-D-SH starts at $E_{red(onset)}$ = −1.40 V (vs Fc/Fc^+). Its oxidation of begins at $E_{ox(onset)}$ = 0.87 V (vs Fc/Fc^+). The EA and IP values, calculated on the basis of the electrochemical data, are −3.40 and 5.70 eV, respectively. These values yield the electrochemical band gap, Eg_{el} = 2.30 eV.

In Figure 6 absorption and emission spectra of D-A-D-SH are presented. The absorption band peaked at 399 nm is inhomogeneously broadened toward longer wavelengths. Its optical band gap, Eg_{opt}, is equal to 2.60 eV. D-A-D-SH is a rather weak luminophore (QY = 2.5%); its large Stoke shift of 126 nm should be noted, since the emission band shows its maximum at 525 nm. Compared to D-A-D-SH, before introduction of an −SH group, the D-A-D emitted blue light (λ_{max} = 473 nm, QY = 10%; see Figure S11).

The next question to be considered is how the electrochemical and spectroscopic properties of $Ag_{1.0}In_{3.1}Zn_{1.0}S_{4.0}(S_{6.1})$ and D-A-D-SH are altered upon the formation of their hybrid. Figure 7 presents a representative

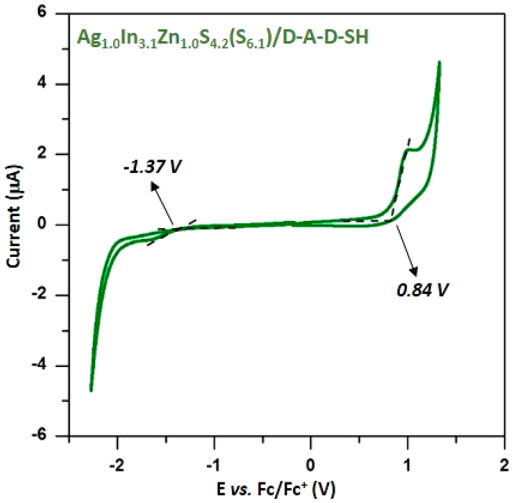

Figure 7. Cyclic voltammograms of $Ag_{1.0}In_{3.1}Zn_{1.0}S_{4.2}(S_{6.1})$ nanocrystals capped with ligand (D-A-D-SH). Electrolyte: 0.1 M Bu_4NBF_4/CH_2Cl_2, reference electrode Ag/0.1 M $AgNO_3$ in acetonitrile, scan rate = 50 mV/s.

cyclic voltammogram of the Ag−In−Zn−S/D-A-D-SH hybrid. The potential of the oxidation onset (0.84 V vs Fc/Fc^+) is only slightly lowered (by 30 mV) with respect to the corresponding potential registered for the free ligand. This strongly indicates that the oxidation process takes place at the organic (ligand) part of the hybrid. On the other hand, the potential of the reduction process onset is only slightly higher (by 30 mV) than that of the free ligand. Ionization potential and electron affinity of the hybrid were calculated according to eqs 1 and 2, yielding the following values: EA = −3.43 eV, IP = 5.64 eV, and Eg_{el} = 2.20 eV. Thus, the exchange of initial ligands for D-A-D-SH lowered the band gap by 0.60 eV.

The UV−vis−NIR spectrum of the hybrid is dominated by the absorption peak originating from the D-A-D-SH ligand which is very similar to the corresponding peak of the free ligand as far as its position and shape are concerned (λ_{max} = 399 nm, Eg_{opt} = 2.6 eV; see Figure 6). The most pronounced effect induced by the ligand exchange concerns the photoluminescence. As already mentioned, $Ag_{1.0}In_{3.1}Zn_{1.0}S_{4.0}(S_{6.1})$ nanocrystals are efficient luminophores emitting red light (λ_{max} = 720 nm, QY = 67%). Upon exchange of primary ligands for D-A-D-SH this red photoluminescence is totally quenched, and new green photoluminescence appears (λ_{max} = 508 nm), originating from the ligand. The emission peak is slightly hypsochromically shifted as compared to the corresponding peak of the free ligand. Its QY = 10% is 4-fold higher than QY of free D-A-D-SH ligands. To determine the mechanism of the observed changes, the emission spectra for complexes of D-A-D-SH ligand with Ag^+, In^{3+}, and Zn^{2+} cations were recorded. The complexes were obtained by adding the solution of the ligand in toluene to the appropriate salts ($AgNO_3$, $InCl_3$, and zinc stearate). Comparing the emission spectrum of the free ligand with those recorded for the formed complexes, a change in the position of the emission peak could be observed (see Figure S12). Only in the case of the D-A-D-SH complex with Ag^+ partial extinction of the emission was detected. The performed studies indicated that luminescent properties of the Ag−In−Zn−S/D-A-D-SH hybrid were a result of interactions between the nanocrystal and the ligand. Thus, they did not originate from the formation of bonds between the ligands and specific surfacial cations of the nanocrystal.

Results of electrochemical and spectroscopic investigations obtained for $Ag_{1.0}In_{3.1}Zn_{1.0}S_{4.0}(S_{6.1})$ capped with initial ligands, free ligand D-A-D-SH and $Ag_{1.0}In_{3.1}Zn_{1.0}S_{4.2}(S_{6.1})$/D-A-D-SH hybrid, are summarized in Table 1.

To explain the effect of the emission color change upon introducing D-A-D-SH ligands to $Ag_{1.0}In_{3.1}Zn_{1.0}S_{4.0}(S_{6.1})$, it is instructive to briefly discuss the already-mentioned donor−acceptor mechanism of radiative recombination 1S(e) → 1S(h) in nonstoichiometric Ag−In−Zn−S nanocrystals capped with optically and electrochemically inactive primary ligands. The photoluminescence QY is in this case strongly related to the presence of point defects in the inorganic core which favor the emission. These are Ag vacancies (V_{Ag}) and S interstitials (S_i) as acceptor levels and S vacancies (V_S) and Ag interstitials (Ag_i) as donor levels.[74,75] These donor and acceptor levels act as traps for charge carriers leading in the next step to radiative

Table 1. Redox Potentials (vs Fc/Fc^+), Electrochemically Determined Ionization Potential (IP) and Electron Affinity (EA), Electrochemical and Optical Band Gaps, Maxima of the Photoluminescence Bands (PL), Quantum Yields (QY) for Ag−In−Zn−S Nanocrystals Capped with Initial Ligands, D-A-D-SH and the Hybrid, i.e., Ag−In−Zn−S Nanocrystals Capped with Ligand D-A-D-SH

	E^{ox}_{onset} (V) (Fc/Fc^+)	E^{red}_{onset} (V) (Fc/Fc^+)	IP (eV)	EA (eV)	Eg_{el} (eV)	Eg_{opt} (eV)	PL (nm)	QY (%)
AgInZnS	1.28	−1.49	6.1	−3.3	2.8	2.6	720	67.0
D-A-D-SH	0.87	−1.40	5.7	−3.4	2.3	2.6	525	2.5
hybrid	0.84	−1.37	5.6	−3.4	2.2	2.6	508	10.0

https://dx.doi.org/10.1021/acs.inorgchem.0c02468
Inorg. Chem. 2020, 59, 14594−14604

recombination, which is significantly lower in energy than the band gap.[72,76−81]

In $Ag_{1.0}In_{3.1}Zn_{1.0}S_{4.0}(S_{6.1})$ nanocrystals capped with initial ligands are characterized by the Ag/In ∼ 0.3 and a strong deficit of sulfur (compare to the experimentally determined sulfur content ($S_{4.0}$) and the theoretical one calculated for the determined content of metals ($S_{6.1}$)). This nanocrystal composition should result in the presence of appropriate donor and acceptor states favoring the above-mentioned donor−acceptor radiative recombination mechanism. This reasoning is fully consistent with the spectroscopic results. Their spectroscopically determined Eg_{opt} is equal to 2.6 eV, whereas their luminescence band is peaked at 720 nm (red light) and is characterized by a large Stokes shift (∼170 nm), a large FWHM value (∼150 nm), and a high photoluminescence QY (67%). The observed radiative recombination involving donor and acceptor states corresponds to ΔE ∼ 1.7 eV. This is schematically presented in Figure 8a where IP and EA are converted to HOMO and LUMO, according to Koopmans' theorem.

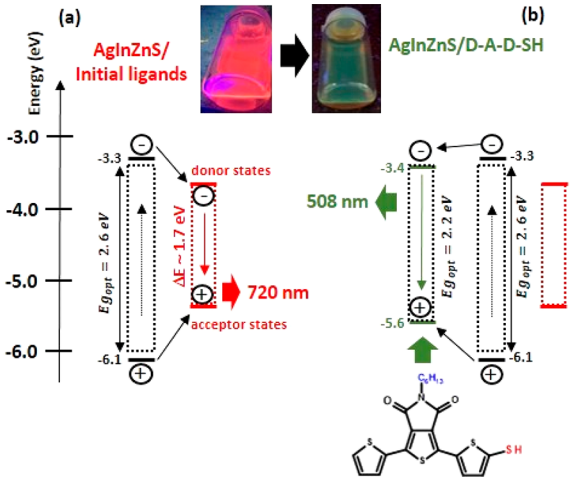

Figure 8. Photoluminescence mechanisms in alloyed Ag−In−Zn−S nanocrystals capped with initial ligands (a) and electroactive ligands (D-A-D-SH) (b).

Upon exchange of inactive primary ligands for D-A-D-SH, a distinct change of the emission color from red (720 nm) to green (508 nm) occurs, indicating that the ligand states are involved in the emission. The emission band is hypsochromically shifted by 17 nm as compared to the corresponding band of the free ligand. The red emission characteristic of nanocrystals capped with primary ligands is totally quenched. The exchange of inactive primary ligands for D-A-D-SH introduces additional states located at −3.4 and −5.6 eV, that is, below the $Ag_{1.0}In_{3.1}Zn_{1.0}S_{4.0}(S_{6.1})$ nanocrystals' LUMO level and above their HOMO level, respectively. Thus, ligand states can act as traps for photogenerated charge carriers. Therefore, in addition to direct ligand excitation as in free D-A-D-SH, another photoluminescence mechanism is envisioned involving charge and energy transfer from the inorganic core to the ligand as schematically depicted in Figure 8b. The above outlined mechanism is corroborated by the excitation spectra recorded for D-A-D-SH, Ag−In−Zn−S nanocrystals capped with initial ligands, and the Ag−In−Zn−S/D-A-D-SH hybrid (see Figure S13). The excitation spectrum of nanocrystals capped with initial ligands is broad and has a rather complex shape with a clear maximum at ∼580 nm and a shoulder near ∼440 nm, coinciding with the onset of the increasing absorbance in the spectrum of Ag−In−Zn−S stabilized with primary ligands. The excitation spectrum of free D-A-D-SH is characterized by a rather narrow band peaked at 330 nm. The corresponding excitation spectrum of Ag−In−Zn−S/D-A-D-SH hybrid consists of two narrow peaks at 340 and 440 nm; the first one nearly coincides with the corresponding peak of the free ligand, whereas the second one closely matches the absorption spectrum of the hybrid (compare Figure 6 and Figure S13). Thus, these spectroscopic investigations clearly indicate that two mechanisms are involved in the luminescence generation in Ag−In−Zn−S/D-A-D-SH nanocrystals—direct excitation of the ligand and the excitation of nanocrystals followed by the energy transfer from the nanocrystal to the ligand, as schematically depicted in Figure 8b. An evident manifestation of this additional mechanism is a 4-fold increase of QY from 2.5% in free D-A-D-SH to 10% in the nanocrystal surface bound ligands.

Moreover, for Ag−In−Zn−S capped with initial ligands, the free D-A-D-SH ligand and the hybrid (Ag−In−Zn−S/D-A-D-SH) photoluminescence decay profiles were recorded (see Figure S14). The decay curves (λ_{exc} = 405 nm) were multiexponential in nature. They could be fitted via the following equation:

$$I(t) = A_1 \exp\left\{-\frac{t}{\tau_1}\right\} + A_2 \exp\left\{-\frac{t}{\tau_2}\right\} \quad (3)$$

where τ_1 and τ_2 represent the decay time of the photoluminescence and A_1 and A_2 (Table 2) represent the relative weight of the decay components at t = 0.[82−84] Based on the performed calculations, Ag−In−Zn−S nanocrystals capped with initial ligands were characterized by a relatively long average photoluminescence lifetime of 1227 ns, that is, in the range typical of stoichiometric $AgInS_2$ and alloyed $AgInS_2$−ZnS nanocrystals.[72,85] However, in the case of free D-A-D-SH ligands and the Ag−In−Zn−S/D-A-D-SH hybrid, significantly shorter and practically the same values of the photoluminescence lifetime (0.59 and 0.57 ns, respectively) were obtained, unequivocally proving a change in the photoluminescence mechanism occurring upon the exchange of the primary ligands for D-A-D-SH (Figure 8b).

Table 2. Biexponential Fitting Results for Photoluminescence Decay Profiles of Ag−In−Zn−S Nanocrystals Capped with Initial Ligands, 2-(5-Mercaptothien-2-yl)-8-(thien-2-yl)-5-hexylthieno[3,4-*c*]pyrrole-4,6-dione (D-A-D-SH), and Ag−In−Zn-S/D-A-D-SH Hybrid

	τ_1 (ns)	A_1 (%)	τ_2 (ns)	A_2 (%)	lifetime (ns)
AgInZnS	677.82	56.82	1949.82	43.18	1227.00
D-A-D-SH	0.53	95.60	1.94	4.40	0.59
hybrid	0.52	96.08	1.75	3.92	0.57

It should be noted that the observed luminescence color change is inherently associated with the presence of the D-A-D- unit since optically inactive ligands with an −*SH* anchor group cause only minimal changes in emission spectra of nonstoichiometric Ag−In−Zn−S nanocrystals.[34,35,39]

https://dx.doi.org/10.1021/acs.inorgchem.0c02468
Inorg. Chem. 2020, 59, 14594−14604

CONCLUSIONS

The donor−acceptor−donor semiconductor compound, namely 2-(5-mercaptothien-2-yl)-8-(thien-2-yl)-5-hexylthieno-[3,4-*c*]pyrrole-4,6-dione (abbreviated as D-A-D-SH), was designed, synthesized, and used as a capping ligand in nonstoichiometric Ag−In−Zn−S nanocrystals. D-A-D-SH is a weak luminophore emitting green light (λ_{max} = 525 nm, QY = 2.5%). Despite limited solubility, it readily exchanges nanocrystals initial ligands (stearic acid and 1-aminooctadecane). Binding D-A-D-SH to the nanocrystals surface changes its polarity improving the colloidal stability of the obtained $Ag_{1.0}In_{3.1}Zn_{1.0}S_{4.2}(S_{6.1})$/D-A-D-SH hybrid. It also profoundly changes the luminescent properties of the system. Efficient red luminescence, characteristic of nanocrystals capped with initial ligands (λ_{max} = 720 nm, QY = 67%), is totally quenched, and green luminescence originating from the ligands appears at 508 nm, exhibiting a 4-fold increase QY value (10%) as compared to that of free D-A-D-SH. This luminescence can proceed by two pathways: (i) by direct excitation of the ligand as in the case of free D-A-D-SH or (ii) by charge and energy transfer from the nanocrystal core to the new states introduced to the system through surface binding of the optically active ligand.

EXPERIMENTAL SECTION

Materials. *N*-Bromosuccinimide (NBS, 99%), thiophene-2-boronic acid pinacol ester (98%), $Pd(PPh_3)_4$ (99%), K_2CO_3 (99%), NH_4SCN (97%), bromodimethylsulfonium bromide (95%), tributylphosphine (97%), acetonitrile (99%), butyl acetate (99%), *N*,*N*-dimethylformamide (99%), and benzene-d_6 (100%, 99.6 atom % D) were supplied by Sigma-Aldrich.

Preparation of 2,8-Dibromo-5-(*n*-hexyl)thieno[3,4-*c*]-pyrrole-4,6-dione (6).[54] 5-(*n*-Hexyl)thieno[3,4-*c*]pyrrole-4,6-dione (TPD) (0.66 g, 2.8 mmol) was dissolved in 4.0 mL of concentrated sulfuric acid and 13.0 mL of trifluoroacetic acid. *N*-Bromosuccinimide (NBS) (1.42 g, 8.0 mmol) was added in one portion, and the reaction mixture was stirred for 12 h at room temperature. The brown solution was then diluted with 200 mL of water and extracted with dichloromethane. The organic phase was dried over anhydrous magnesium sulfate and evaporated to afford the crude product as orange crystals. Purification by column chromatography using silica gel and toluene/dichloromethane/heptane (3:3:1) as eluent followed by recrystallization from aqueous ethanol gave 2,8-dibromo-5-(*n*-hexyl)thieno[3,4-*c*]pyrrole-4,6-dione (0.99 g, 2.5 mmol, 90%) as white crystals.

2,8-Bis(thien-2-yl)-5-(*n*-hexyl)thieno[3,4-*c*]pyrrole-4,6-dione (D-A-D). D-A-D was obtained by using a modification of procedures described in ref 56. A mixture of 2,8-dibromo-5-(*n*-hexyl)thieno[3,4-*c*]pyrrole-4,6-dione (1.48 g, 3.0 mmol), thiophene-2-boronic acid pinacol ester (2.30 g, 6.2 mmol), $Pd(PPh_3)_4$ (0.35 g, 7.5 mmol), K_2CO_3 (2.76 g, 20 mmol), and DMF (45 mL) was stirred at 110 °C for 2 h under an argon atmosphere. After cooling to room temperature, the reaction mixture was poured into saturated sodium chloride solution (60 mL) and then extracted with ethyl acetate (2 × 60 mL). The combined organic extracts were washed with water and dried over anhydrous sodium sulfate. After the solvent was removed, the residue was purified by column chromatography on silica gel with hexane/ethyl acetate (v/v 25/1 to 9/1) as eluent to give D-A-D as a green solid (0.78 g, 1.9 mmol, 65%). ^{1}H NMR (400 MHz, C_6D_6): δ = 0.83 ppm (t, J = 6.9 Hz, 3H, CH_3), 1.14−1.25 (m, 6H, 3 × CH_2), 1.57−1.65 (m, 2H, $C\underline{H}_2CH_2N$), 3.55 (t, J = 7.4 Hz, 2H, CH_2N), 6.65 (dd, J = 5.0 Hz, J = 3.8 Hz, 2H, 2 × CH), 6.73 (dd, J = 5.0 Hz, J = 1.0 Hz, 2H, 2 × CH), 8.13 (dd, J = 3.8 Hz, J = 1.0 Hz, 2H, 2 × CH). ^{13}C NMR (100 MHz, C_6D_6): δ = 14.2 ppm (CH_3), 22.9 (CH_2), 26.9 (CH_2), 28.9 (CH_2), 31.7 (CH_2), 38.6 (CH_2N), 127.8 (2 × CH), 128.2 (2 × CH), 129.5 (2 × C), 130.2 (2 × CH), 133.1 (2 × C), 136.0 (2 × C), 162.4 (C═O).

2-(5-Thiocyanatothien-2-yl)-8-(thien-2-yl)-5-hexylthieno-[3,4-*c*]pyrrole-4,6-dione (7). 7 was obtained by using a modification of procedures described in ref 57. 2,8-Bis(thien-2-yl)-5-(*n*-hexyl)thieno[3,4-*c*]pyrrole-4,6-dione (1.25 g, 3.13 mmol) was dissolved in 60 mL of anhydrous acetonitrile and 15 mL of chloroform. NH_4SCN (0.36 g, 4.7 mmol) and bromodimethylsulfonium bromide (0.74 g, 3.1 mmol) were added, and the reaction mixture was stirred at room temperature for 9 days under an argon atmosphere. After removing the solvents the residue was dissolved in chloroform (100 mL), washed with water, dried over anhydrous sodium sulfate, evaporated, and dried under vacuum. The crude product was purified by column chromatography on silica gel with chloroform to chloroform/methanol (v/v 10/1) as eluent to give a thiocyanato product (0.77 g, 1.7 mmol, 54%) *Caution! Reaction generates odorous dimethyl sulfide. All operations should be performed in a well-ventilated hood. The effluent should be treated with bleach before disposal.*

2-(5-Mercaptothien-2-yl)-8-(thien-2-yl)-5-hexylthieno[3,4-*c*]pyrrole-4,6-dione (D-A-D-SH). D-A-D-SH was obtained by using a modification of procedures described in ref 58. To a solution of 2-(5-thiocyanatothien-2-yl)-8-(thien-2-yl)-5-hexylthieno[3,4-*c*]pyrrole-4,6-dione (0.53 g, 1.15 mmol) in acetone (75 mL) and water (0.3 mL) tributylphosphine (0.5 mL, 2.30 mmol) was added dropwise. After stirring for 10 min, 3 mL of water and 1 mL of aqueous HCl (10%) were added. The resulting reaction mixture was stirred at room temperature overnight. After the solvents were removed, the residue was dissolved in chloroform (100 mL), washed with water, dried over anhydrous sodium sulfate, evaporated, and dried under vacuum. Purification was performed by column chromatography using silica gel and chloroform to chloroform/methanol (v/v, 10/1) as eluent followed by recrystallization from butyl acetate gave 2-(5-mercaptothien-2-yl)-8-(thien-2-yl)-5-hexylthieno[3,4-*c*]pyrrole-4,6-dione (0.24 g, 0.55 mmol, 48%) as orange crystals. ^{1}H NMR (400 MHz, C_6D_6): δ = 0.84 ppm (t, J = 6.9 Hz, 3H, CH_3), 1.14−1.25 (m, 6H, 3 × CH_2), 1.57−1.64 (m, 2H, $C\underline{H}_2CH_2N$), 3.53 (t, J = 7.4 Hz, 2H, CH_2N), 6.64 (dd, J = 5.0 Hz, J = 3.8 Hz, 1H, CH), 6.74 (dd, J = 5.0 Hz, J = 1.0 Hz, 1H, CH), 6.93 (d, J = 3.9 Hz, 1H, CH), 7.87 (d, J = 3.9 Hz, 1H, CH), 8.11 (dd, J = 3.8 Hz, J = 1.0 Hz, 1H, CH).

Exchange of Initial Ligands for 2-(5-Mercaptothien-2-yl)-8-(thien-2-yl)-5-hexylthieno[3,4-*c*]pyrrole-4,6-dione (D-A-D-SH). A mixture consisting of colloidal solution of Ag−In−Zn−S nanocrystals capped with initial ligands (~200 mg in 10 mL of toluene) and D-A-D-SH (100 mg, 0.23 mmol) was stirred at room temperature for 12 h. The nanocrystals were precipitated with acetone, centrifuged, and redispersed in toluene (or hexane, chloroform, or dichloromethane). The use of a large excess of D-A-D-SH resulted in binding of the largest number of the target ligands to the nanocrystals surface and assured the reproducibility of the optical and electrochemical properties of the resulting hybrids.

ASSOCIATED CONTENT

Supporting Information

The Supporting Information is available free of charge at https://pubs.acs.org/doi/10.1021/acs.inorgchem.0c02468.

Preparation of alloyed Ag−In−Zn−S nanocrystals, synthesis of thieno[3,4-*c*]pyrrole-4,6-dione (TPD), characterization methods, XPS spectra and HR-TEM image of Ag−In−Zn−S nanocrystals capped with initial ligands, EDS spectra and TEM images of Ag−In−Zn−S nanocrystals capped with initial ligands and D-A-D-SH, ^{1}H,^{13}C, and ^{1}H−^{1}H COSY and ^{1}H−^{13}C HMQC NMR spectra recorded for the initial ligands, D-A-D, D-A-D-SH, and Ag−In−Zn−S/D-A-D-SH hybrid, band gap calculation, UV−vis−NIR and photoluminescence spectra of D-A-D, photoluminescence excitation and decay curves of D-A-D-SH and Ag−In−Zn−S nanocrystals capped with initial ligands and D-A-D-SH (PDF)

https://dx.doi.org/10.1021/acs.inorgchem.0c02468
Inorg. Chem. 2020, 59, 14594−14604

AUTHOR INFORMATION

Corresponding Authors

Patrycja Kowalik − *Faculty of Chemistry, Warsaw University of Technology, 00-664 Warsaw, Poland; Faculty of Chemistry, University of Warsaw, PL-02-093 Warsaw, Poland*; Email: pkowalik@ch.pw.edu.pl

Piotr Bujak − *Faculty of Chemistry, Warsaw University of Technology, 00-664 Warsaw, Poland*; orcid.org/0000-0003-2162-961X; Email: piotrbujakchem@poczta.onet.pl

Authors

Zbigniew Wróbel − *Institute of Organic Chemistry, Polish Academy of Sciences, 01-224 Warsaw, Poland*

Mateusz Penkala − *Institute of Chemistry, Faculty of Science and Technology, University of Silesia, 40-007 Katowice, Poland*

Kamil Kotwica − *Faculty of Chemistry, Warsaw University of Technology, 00-664 Warsaw, Poland; Institute of Physical Chemistry, Polish Academy of Sciences, 01-224 Warsaw, Poland*

Anna Maroń − *Institute of Chemistry, Faculty of Science and Technology, University of Silesia, 40-007 Katowice, Poland*

Adam Pron − *Faculty of Chemistry, Warsaw University of Technology, 00-664 Warsaw, Poland*

Complete contact information is available at: https://pubs.acs.org/10.1021/acs.inorgchem.0c02468

Author Contributions

P.K. and P.B. designed the concepts; P.K., Z.W., M.P., K.K., and A.M. performed the experiments; P.K., M.P., and P.B. discussed the results; P.K., P.B., and A.P. supervised the manuscript.

Notes

The authors declare no competing financial interest.

ACKNOWLEDGMENTS

This work was supported by the National Science Centre of Poland, Grant 2015/17/B/ST4/03837. P.K. additionally acknowledges financial support from the Project TRI-BIO-CHEM which is implemented under the Operational Program Knowledge Education Development 2014-2020 cofinanced by the European Social Fund. M.P. and A.M. acknowledge partial support of the University of Silesia.

REFERENCES

(1) Talapin, D. V.; Lee, J.-S.; Kovalenko, M. V.; Shevchenko, E. V. Prospects of Colloidal Nanocrystals for Electronic and Optoelectronic Applications. *Chem. Rev.* **2010**, *110*, 389−458.

(2) Reiss, P.; Couderc, E.; De Girolamo, J.; Pron, A. Conjugated Polymers/Semiconductor Nanocrystals Hybrid Materials − Preparation, Electrical Transport Properties and Applications. *Nanoscale* **2011**, *3*, 446−489.

(3) Palui, G.; Aldeek, F.; Wang, W.; Mattoussi, H. Strategies for Interfacing Inorganic Nanocrystals with Biological Based on Polymer-Coating. *Chem. Soc. Rev.* **2015**, *44*, 193−227.

(4) Jing, L.; Kershaw, S. V.; Li, Y.; Huang, X.; Li, Y.; Rogach, A. L.; Gao, M. Aqueous Based Semiconductor Nanocrystals. *Chem. Rev.* **2016**, *116*, 10623−10730.

(5) Reiss, P.; Carrière, M.; Lincheneau, C.; Vaure, L.; Tamang, S. Synthesis of Semiconductor Nanocrystals, Focusing on Nontoxic and Earth-Abundant Materials. *Chem. Rev.* **2016**, *116*, 10731−10819.

(6) Coughlan, C.; Ibáñez, M.; Dobrozhan, O.; Singh, A.; Cabot, A.; Ryan, K. M. Compound Copper Chalcogenide Nanocrystals. *Chem. Rev.* **2017**, *117*, 5865−6109.

(7) Sobiech, M.; Bujak, P.; Luliński, P.; Pron, A. Semicondutor Nanocrystal-Polymer Hybrid Nanomaterials and their Application in Molecular Imprinting. *Nanoscale* **2019**, *11*, 12030−12074.

(8) Moodelly, D.; Kowalik, P.; Bujak, P.; Pron, A.; Reiss, P. Synthesis, Photophysical Properties and Surface Chemistry of Chalcopyrite-Type Semiconductor Nanocrystals. *J. Mater. Chem. C* **2019**, *7*, 11665−11709.

(9) Jasieniak, J.; Califano, M.; Watkins, S. E. Size-Dependent Valence and Conduction Band-Edge Energies of Semiconductor Nanocrystals. *ACS Nano* **2011**, *5*, 5888−5902.

(10) Voznyy, O.; Zhitomirsky, D.; Stadler, P.; Ning, Z.; Hoogland, S.; Sargent, E. H. A Charge-Orbital Balance Picture of Doping in Colloidal Quantum Dot Solids. *ACS Nano* **2012**, *6*, 8448−8455.

(11) Brown, P. R.; Kim, D.; Lunt, R. R.; Zhao, N.; Bawendi, M. G.; Grossman, J. C.; Bulović, V. Energy Level Modification in Lead Sulfide Quantum Dot Thin Films through Ligand Exchange. *ACS Nano* **2014**, *8*, 5863−5872.

(12) Ning, Z.; Dong, H.; Zhang, Q.; Voznyy, O.; Sargent, E. H. Solar Cells Based on Inks of n-Type Colloidal Quantum Dots. *ACS Nano* **2014**, *8*, 10321−10327.

(13) Yuan, M.; Liu, M.; Sargent, E. H. Colloidal Quantum Dot Solids for Solution-Processed Solar Cells. *Nat. Energy* **2016**, *1*, 16016.

(14) Calzada, R.; Thompson, C. M.; Westmoreland, D. E.; Edme, K.; Weiss, E. A. Organic-to-Aqueous Phase Transfer of Cadmium Chalcogenide Quantum Dots Using a Sulfur-Free Ligand for Enhanced Photoluminescence and Oxidative Stability. *Chem. Mater.* **2016**, *28*, 6716−6723.

(15) Witt, E.; Witt, F.; Trautwein, N.; Fenske, D.; Neumann, J.; Borchert, H.; Parisi, J.; Kolny-Olesiak, J. Synthesis of Lead Chalcogenide Nanocrystals and Study of Charge Transfer in Blends of PbSe Nanocrystals and Poly(3-hexylthiophene). *Phys. Chem. Chem. Phys.* **2012**, *14*, 11706−11714.

(16) Lin, H.; Wu, Y.; Cao, X.; Fu, H. Engineering of Interfacial Electron Transfer from Donor-Acceptor Type Organic Semiconductor to ZnO Nanorod for Visible-Light Detection. *J. Phys. Chem. C* **2012**, *116*, 21657−21663.

(17) Krause, C.; Miranti, R.; Witt, F.; Neumann, J.; Fenske, D.; Parisi, J.; Borchert, H. Charge Transfer and Recombination in Organic/Inorganic Hybrid Composites with $CuInS_2$ Nanocrystals Studied by Light-Induced Electron Spin Resonance. *Sol. Energy Mater. Sol. Cells* **2014**, *124*, 241−246.

(18) Lefrançois, A.; Luszczynska, B.; Pepin-Donat, B.; Lombard, C.; Bouthinon, B.; Verilhac, J.-M.; Gromova, M.; Faure-Vincent, J.; Pouget, S.; Chandezon, F.; Sadki, S.; Reiss, P. Enhanced Charge Separation in Ternary P3HT/PCBM/$CuInS_2$ Nanocrystals Hybrid Solar Cells. *Sci. Rep.* **2015**, *5*, 7768.

(19) Oh, S.; Yang, M.; Kang, S.; Chung, S.-H.; Bouffard, J.; Hong, S.; Park, S.-J. Binary Self-Assembly of Conjugated Block Copolymers and Quantum Dots at the Air-Liquid Interface into Ordered Functional Nanoarrays. *ACS Appl. Mater. Interfaces* **2019**, *11*, 28538−28545.

(20) Harris, R. D.; Bettis Homan, S.; Kodaimati, M.; He, C.; Nepomnyashchii, A. B.; Swenson, N. K.; Lian, S.; Calzada, R.; Weiss, E. A. Electronic Processes within Quantum Dot-Molecule Complexes. *Chem. Rev.* **2016**, *116*, 12865−12919.

(21) Park, Y.; Advincula, R. C. Hybrid Semiconductor Nanoparticles: π-Conjugated Ligands and Nanostructured Films. *Chem. Mater.* **2011**, *23*, 4273−4294.

(22) Pron, A.; Gawrys, P.; Zagorska, M.; Djurado, D.; Demadrille, R. Electroactive Materials for Organic Electronics: Preparation Strategies Structural Aspects and Characterization Techniques. *Chem. Soc. Rev.* **2010**, *39*, 2577−2632.

(23) Lin, Y.; Li, Y.; Zhan, X. Small Molecule Semiconductors for High-Efficiency Organic Photovoltaics. *Chem. Soc. Rev.* **2012**, *41*, 4245−4272.

(24) Bujak, P.; Kulszewicz-Bajer, I.; Zagorska, M.; Maurel, V.; Wielgus, I.; Pron, A. Polymers for Electronics and Spintronics. *Chem. Soc. Rev.* **2013**, *42*, 8895−8999.

(25) Liu, J.; Tanaka, T.; Sivula, K.; Alivisatos, A. P.; Frechet, J. M. J. Employing End-Functional Polythiophene To Control the Morphol-

ogy of Nanocrystal − Polymer Composites in Hybrid Solar Cells. *J. Am. Chem. Soc.* **2004**, *126*, 6550−6551.
(26) Kim, E.; Ruankham, P.; Lee, J.-H.; Hachiya, K.; Sagawa, T. Ag-In-Zn-S Quantum Dots for Hybrid Organic-Inorganic Solar Cells. *Jpn. J. Appl. Phys.* **2016**, *55*, 02BF06.
(27) Kobosko, S. M.; Jara, D. H.; Kamat, P. V. $AgInS_2$-ZnS Quantum Dots: Excited State Interactions with TiO_2 and Photovoltaic Performance. *ACS Appl. Mater. Interfaces* **2017**, *9*, 33379−33388.
(28) Ji, C.; Lu, M.; Wu, H.; Zhang, X.; Shen, X.; Wang, X.; Zhang, Y.; Wang, Y.; Yu, W. W. 1,2-Ethanedithiol Treatment for $AgIn_5S_8$/ZnS Quantum Dot Light-Emitting Diodes with High Brightness. *ACS Appl. Mater. Interfaces* **2017**, *9*, 8187−8193.
(29) Choi, D. B.; Kim, S.; Yoon, H. C.; Ko, M.; Yang, H.; Do, Y. R. Color-Tunable Ag-In-Zn-S Quantum-Dot Light-Emitting Devices Realizing Green, Yellow and Amber Emissions. *J. Mater. Chem. C* **2017**, *5*, 953−959.
(30) Lee, S. J.; Kim, Y.; Jung, J.; Kim, M. A.; Kim, N.; Lee, S. J.; Kim, S. K.; Kim, Y.-R.; Park, J. K. Rapid and Facile Synthesis of a $(Zn_xAg_yIn_z)S_2$ Nanocrystal Library *via* Sono-Combichem Method and its Characterization Including Single Nanocrystal Analysis. *J. Mater. Chem.* **2012**, *22*, 11957−11963.
(31) Subramaniam, P.; Lee, S. J.; Shah, S.; Patel, S.; Starovoytov, V.; Lee, K.-B. Generation of a Library of Non-Toxic Quantum Dots for Cellular Imaging and sRNA Delivery. *Adv. Mater.* **2012**, *24*, 4014−4019.
(32) Xuan, T.-T.; Liu, J.-Q.; Yu, C.-Y.; Xie, R.-J.; Li, H.-L. Facile Synthesis of Cadmium-Free Zn-In-S:Ag/ZnS Nanocrystals for Bio-Imaging. *Sci. Rep.* **2016**, *6*, 24459.
(33) Ogihara, Y.; Yukawa, H.; Kameyama, T.; Nishi, H.; Onoshima, D.; Ishikawa, T.; Torimoto, T.; Baba, Y. Labeling and in vivo visualization of Transplanted Adipose Tissue-Derived Stem Cells with Safe Cadmium-Free Aqueous ZnS Coating of ZnS-$AgInS_2$ Nanoparticles. *Sci. Rep.* **2017**, *7*, 40047.
(34) Matysiak-Brynda, E.; Bujak, P.; Augustin, E.; Kowalczyk, A.; Mazerska, Z.; Pron, A.; Nowicka, A. M. Stable Nanoconjugates of Transferrin with Alloyed Quaternary Nanocrystals Ag-In-Zn-S as a Biological Entity for Tumor Recognition. *Nanoscale* **2018**, *10*, 1286−1296.
(35) Pilch, J.; Matysiak-Brynda, E.; Kowalczyk, A.; Bujak, P.; Mazerska, Z.; Nowicka, A. M.; Augustin, E. Quaternary Quantum Dots Conjugated with New Unsymmetrical Bisacridine Derivatives Improve Cancer Therapy *via* Enhancing Cytotoxicity Towards Cancer Cells and Protecting Normal Cells. *ACS Appl. Mater. Interfaces* **2020**, *12*, 17276−17289.
(36) Zhong, H.; Bai, Z.; Zou, B. Tuning the Luminescence Properties of Colloidal I-III-VI Semiconductor Nanocrystals for Optoelectronics and Biotechnology Applications. *J. Phys. Chem. Lett.* **2012**, *3*, 3167−3175.
(37) Gabka, G.; Bujak, P.; Giedyk, K.; Ostrowski, A.; Malinowska, K.; Herbich, J.; Golec, B.; Wielgus, I.; Pron, A. A Simple Route to Alloyed Quaternary Nanocrystals Ag-In-Zn-S with Shape and Size Control. *Inorg. Chem.* **2014**, *53*, 5002−5012.
(38) Gabka, G.; Bujak, P.; Kotwica, K.; Ostrowski, A.; Lisowski, W.; Sobczak, J. W.; Pron, A. Luminophores of Tunable Colors from Ternary Ag-In-S and Quaternary Ag-In-Zn-S Nanocrystals Covering the Visible to Near-Infrared Spectral Range. *Phys. Chem. Chem. Phys.* **2017**, *19*, 1217−1228.
(39) Bujak, P.; Wróbel, Z.; Penkala, M.; Kotwica, K.; Kmita, A.; Gajewska, M.; Ostrowski, A.; Kowalik, P.; Pron, A. Highly Luminescent Ag-In-Zn-S Quaternary Nanocrystals: Growth Mechanism and Surface Chemistry Elucidation. *Inorg. Chem.* **2019**, *58*, 1358−1370.
(40) Gabka, G.; Bujak, P.; Gryszel, M.; Kotwica, K.; Pron, A. Anchor Groups Effect on Spectroscopic and Electrochemical Properties of Quaternary Nanocrystals Cu-In-Zn-S Capped with Arylamine Derivatives. *J. Phys. Chem. C* **2015**, *119*, 9656−9664.
(41) Cheng, Y.-J.; Yang, S.-H.; Hsu, C.-S. Synthesis of Conjugated Polymers for Organic Solar Cell Applications. *Chem. Rev.* **2009**, *109*, 5868−5923.
(42) Heeger, A. J. Semiconducting Polymers: the Third Generation. *Chem. Soc. Rev.* **2010**, *39*, 2354−2371.
(43) Lin, Y.; Li, Y.; Zhan, X. Small Molecule Semiconductor for High-Efficiency Organic Photovoltaics. *Chem. Soc. Rev.* **2012**, *41*, 4245−4272.
(44) Wang, H.-Y.; Gao, J.; Gu, L.-J.; Wan, J.-H.; Wei, W.; Liu, F. Structural Modification of Thieno[3,4-*c*]pyrrole-4,6-dione: Structure-Property Relationships and Application in Solution-Processed Small-Molecule Organic Solar Cells. *J. Mater. Chem. A* **2013**, *1*, 5875−5885.
(45) Ha, J.-j.; Kim, Y. J.; Park, J.-g.; An, T. K.; Kwon, S.-K.; Park, C. E.; Kim, Y. H. Thieno[3,4-*c*]pyrrole-4,6-dione-Based Small Molecules for Highly Efficient Solution-Processed Organic Solar Cells. *Chem. - Asian J.* **2014**, *9*, 1045−1053.
(46) Çakal, D.; Ertan, S.; Cihaner, A.; Önal, A. M. Synthesis and Electrochemical Polymerization of D-A-D Type Monomers with Thieno[3,4-*c*]pyrrole-4,6-dione Acceptor Unit. *Dyes Pigm.* **2018**, *158*, 175−182.
(47) Zou, Y.; Najari, A.; Berrouard, P.; Beaupré, S.; Aïch, B. R.; Tao, Y.; Leclerc, M. A Thieno[3,4-*c*]pyrrole-4,6-dione-Based Copolymer for Efficient Solar Cells. *J. Am. Chem. Soc.* **2010**, *132*, 5330−5331.
(48) Piliego, C.; Holcombe, T. W.; Douglas, J. D.; Woo, C. H.; Beaujuge, P. M.; Fréchet, J. M. J. Synthetic Control of Structural Order in N-Alkylthieno[3,4-*c*]pyrrole-4,6-dione-Based Polymers for Efficient Solar Cells. *J. Am. Chem. Soc.* **2010**, *132*, 7595−7597.
(49) Amb, C. M.; Chen, S.; Graham, K. R.; Subbiah, J.; Small, C. E.; So, F.; Reynolds, J. R. Dithienogermole As a Fused Electron Donor in Bulk Heterojunction Solar Cells. *J. Am. Chem. Soc.* **2011**, *133*, 10062−10065.
(50) Chu, T.-Y.; Lu, J.; Beaupré, S.; Zhang, Y.; Pouliot, J.-R.; Wakim, S.; Zhou, J.; Leclerc, M.; Li, Z.; Ding, J.; Tao, Y. Bulk Heterojunction Solar Cells Using Thieno[3,4-c]pyrrole-4,6-dione and Dithieno[3,2-*b*:2′,3′-*d*]silole Copolymer with a Power Conversion Efficiency of 7.3%. *J. Am. Chem. Soc.* **2011**, *133*, 4250−4253.
(51) Najari, A.; Beaupré, S.; Berrouard, P.; Zou, Y.; Pouliot, J.-R.; Lepage-Pérusse, C.; Leclerc, M. Synthesis and Characterization of New Thieno[3,4-*c*]pyrrole-4,6-dione Derivatives for Photovoltaic Applications. *Adv. Funct. Mater.* **2011**, *21*, 718−728.
(52) Jiang, J.-M.; Yuan, M.-C.; Dinakaran, K.; Hariharan, A.; Wei, K.-H. Crystalline Donor-Acceptor Conjugated Polymers for Bulk Heterojunction Photovoltaics. *J. Mater. Chem. A* **2013**, *1*, 4415−4422.
(53) Zhang, Q. T.; Tour, J. M. Alternating Donor/Acceptor Repeat Units in Polythiophenes. Intramolecular Charge Transfer for Reducing Band Gaps in Fully Substituted Conjugated Polymers. *J. Am. Chem. Soc.* **1998**, *120*, 5355−5361.
(54) Nielsen, C. B.; Bjørnholm, T. New Regiosymmetrical Dioxopyrrolo- and Dihydropyrrolo-Functionalized Polythiophenes. *Org. Lett.* **2004**, *6*, 3381−3384.
(55) Berrouard, P.; Grenier, F.; Pouliot, J.-R.; Gagnon, E.; Tessier, C.; Leclerc, M. Synthesis and Characterization of 5-Octylthieno[3,4-*c*]pyrrole-4,6-dione Derivatives As New Monomers for Conjugated Copolymers. *Org. Lett.* **2011**, *13*, 38−41.
(56) Feng, Q.; Zhang, W.; Zhou, G.; Wang, Z.-S. Enhanced Performance of Quasi-Solid-State Dye-Sensitized Solar Cells by Branching the Linear Substituent in Sensitizers Based on Thieno-[3,4-c]pyrrole-4,6-dione. *Chem. - Asian J.* **2013**, *8*, 168−177.
(57) Bhalerao, D. S.; Akamanchi, K. G. Efficient and Novel Method for Thiocyanation of Aromatic and Heteroaromatic Compounds Using Bromodimethylsulfonium Bromide and Ammonium Thiocyanate. *Synlett* **2007**, *2007*, 2952−2956.
(58) Müller, E.; Stegmann, H. B.; Scheffler, K. über Sauerstoffradikale, XXI. Undersuchungen an Schwefelhaltigen Aroxylen Mittels der Elektronenresonanz. *Liebigs Ann. Chem.* **1961**, *645*, 79−91.
(59) Hassinen, A.; Moreels, I.; de Mello Donegá, C.; Martins, J. C.; Hens, Z. Nuclear Magnetic Resonance Spectroscopy Demonstrating

https://dx.doi.org/10.1021/acs.inorgchem.0c02468
Inorg. Chem. 2020, 59, 14594−14604

Dynamic Stabilization of CdSe Quantum Dots by Alkylamines. *J. Phys. Chem. Lett.* **2010**, *1*, 2577−2581.
(60) Hens, Z.; Martins, J. C. A Solution NMR Toolbox for Characterizing the Surface Chemistry of Colloidal Nanocrystals. *Chem. Mater.* **2013**, *25*, 1211−1221.
(61) Arcudi, F.; Westmoreland, D. E.; Weiss, E. A. Colloidally Stable CdS Quantum Dots in Water with Electrostatically Stabilized Weak-Binding, Sulfur-Free Ligands. *Chem. - Eur. J.* **2019**, *25*, 14469−14474.
(62) Coppel, Y.; Spataro, G.; Pagès, C.; Chaudret, B.; Maisonnat, A.; Kahn, M. L. Full Characterization of Collidal Solutions of Long-Alkyl-Chain-Amine-Stabilized ZnO Nanoparticles by NMR Spectroscopy: Surface State, Equilibria, and Affinity. *Chem. - Eur. J.* **2012**, *18*, 5384−5393.
(63) Trasatti, S. The Absolute Electrode Potential: An Explanatory Note. *Pure Appl. Chem.* **1986**, *58*, 955−966.
(64) Querner, C.; Reiss, P.; Sadki, S.; Zagorska, M.; Pron, A. Size and Ligand Effects on the Electrochemical and Spectroelectrochemical Responses of CdSe Nanocrystals. *Phys. Chem. Chem. Phys.* **2005**, *7*, 3204−3209.
(65) Cardona, C. M.; Li, W.; Kaifer, A. E.; Stockdale, D.; Bazan, G. C. Electrochemical Considerations for Determining Absolute Frontier Orbital Energy Levels of Conjugated Polymers for Solar Cell Applications. *Adv. Mater.* **2011**, *23*, 2367−2371.
(66) Amelia, M.; Lincheneau, C.; Silvi, S.; Credi, A. Electrochemical Properties of CdSe and CdTe Quantum Dots. *Chem. Soc. Rev.* **2012**, *41*, 5728−5743.
(67) Sandroni, M.; Wegner, K. D.; Aldakov, D.; Reiss, P. Prospects of Chalcopyrite-Type Nanocrystals for Energy Appllications. *ACS Energy Lett.* **2017**, *2*, 1076−1088.
(68) Shay, J. L.; Tell, B.; Schiavone, L. M.; Kasper, H. M.; Thiel, F. Energy Bands of $AgInS_2$ in the Chalcopyrite and Orthorhombic Structures. *Phys. Rev. B* **1974**, *9*, 1719−1723.
(69) Feng, Z.; Dai, P.; Ma, X.; Zhan, J.; Lin, Z. Monodispersed Cation-Discordered Cubic $AgInS_2$ Nanocrystals with Enhanced Fluorescence. *Appl. Phys. Lett.* **2010**, *96*, 013104.
(70) Wakita, K.; Miyamoto, U.; Paucar, R.; Honjo, K.; Shim, Y.; Tokuda, T.; Yoshino, K. Excitonic Emissions of $AgInS_2$ Crystals with Chalcopyrite and Orthorhombic Structure. *Phys. Status Solidi C* **2013**, *10*, 1042−1045.
(71) Tsuji, I.; Kato, H.; Kobayashi, H.; Kudo, A. Photocatalytic H_2 Evolution Reaction from Aqueous Solutions over Band Structure-Controlled $(AgIn)_xZn_{2(1-x)}S_2$ Solid Solution Photocatalysts with Visible-Light Response and Their Surface Nanostructures. *J. Am. Chem. Soc.* **2004**, *126*, 13406−13413.
(72) Dai, M.; Ogawa, S.; Kameyama, T.; Okazaki, K.-i.; Kudo, A.; Kuwabata, S.; Tsuboi, Y.; Torimoto, T. Tunable Photoluminescence from the Visible to Near-Infrared Wavelength Region of Non-Stoichiometric $AgInS_2$ Nanoparticles. *J. Mater. Chem.* **2012**, *22*, 12851−12858.
(73) Pan, D.; Weng, D.; Wang, X.; Xiao, Q.; Chen, W.; Xu, C.; Yang, Z.; Lu, Y. Alloyed Semiconductor Nanocrystals with Broad Tunable Band Gap. *Chem. Commun.* **2009**, 4221−4223.
(74) Krustok, J.; Raudoja, J.; Krunks, M.; Mändar, H.; Collan, H. Nature of the Native Deep Localized Defect Recombination Centers in the Chalcopyrite and Orthorhombic $AgInS_2$. *J. Appl. Phys.* **2000**, *88*, 205−208.
(75) You, S. H.; Hong, K. J.; Youn, C. J.; Jeong, T. S.; Moon, J. D.; Kim, H. S.; Park, J. S. Origin of Point Defects in $AgInS_2$/GaAs Epilayer Obtained from Photoluminescence Measurement. *J. Appl. Phys.* **2001**, *90*, 3894−3898.
(76) Uehara, M.; Watanabe, K.; Tajiri, Y.; Nakamura, H.; Maeda, H. Synthesis of $CuInS_2$ Fluorescent Nanocrystals and Enhancement of Fluorescence by Controlling Crystal Defect. *J. Chem. Phys.* **2008**, *129*, 134709.
(77) Ogawa, T.; Kuzuya, T.; Hamanaka, Y.; Sumiyama, K. Synthesis of Ag-In Binary Sulfide Nanoparticles-Structural Tuning and Their Photoluminescence Properties. *J. Mater. Chem.* **2010**, *20*, 2226−2231.
(78) Nam, D.-E.; Song, W.-S.; Yang, H. Noninjection, One-Pot Synthesis of Cu-Deficient $CuInS_2$/ZnS Core/Shell Quantum Dots and Their Fluorescent Properties. *J. Colloid Interface Sci.* **2011**, *361*, 491−496.
(79) Mao, B.; Chuang, C.-H.; Wang, J.; Burda, C. Synthesis and Photophysical Properties of Ternary I-III-VI $AgInS_2$ Nanocrystals: Intrinsic versus Surface States. *J. Phys. Chem. C* **2011**, *115*, 8945−8954.
(80) Rao, M. J.; Shibata, T.; Chattopadhyay, S.; Nag, A. Origin of Photoluminescence and XAFS Study of $(ZnS)_{1-x}(AgInS_2)_x$ Nanocrystals. *J. Phys. Chem. Lett.* **2014**, *5*, 167−173.
(81) Chevallier, T.; Le Blevennec, G.; Chandezon, F. Photoluminescence Properties of $AgInS_2$-ZnS Nanocrystals: The Critical Role of the Surface. *Nanoscale* **2016**, *8*, 7612−7620.
(82) Li, L.; Pandey, A.; Werder, D. J.; Khanal, B. P.; Pietryga, J. M.; Klimov, V. I. Efficient Synthesis of Highly Luminescent Copper Indium Sulfide-Based Core/Shell Nanocrystals with Surprisingly Long-Lived Emission. *J. Am. Chem. Soc.* **2011**, *133*, 1176−1179.
(83) Tang, X.; Ho, W. B. A.; Xue, J. M. Synthesis of Zn-Doped $AgInS_2$ Nanocrystals and Their Fluorescence Properties. *J. Phys. Chem. C* **2012**, *116*, 9769−9773.
(84) Kang, X.; Huang, L.; Yang, Y.; Pan, D. Scaling up the Aqueous Synthesis of Visible Light Emitting Multinary $AgInS_2$/ZnS Core/Shell Quantum Dots. *J. Phys. Chem. C* **2015**, *119*, 7933−7940.
(85) Torimoto, T.; Kamiya, Y.; Kameyama, T.; Nishi, H.; Uematsu, T.; Kuwabata, S.; Shibayama, T. Controlling Shape Anisotropy of ZnS-$AgInS_2$ Solid Solution Nanoparticles for Improving Photocatalytic Activity. *ACS Appl. Mater. Interfaces* **2016**, *8*, 27151−27161.

https://dx.doi.org/10.1021/acs.inorgchem.0c02468
Inorg. Chem. 2020, 59, 14594−14604